Dyes and Pigments 89 (2011) 111–119

Contents lists available at ScienceDirect

Dyes and Pigments

journal homepage: www.elsevier.com/locate/dyepig

Syntheses and electrochemical characterization of new water soluble octaarylthiosubstituted manganese phthalocyanines

Irvin Booysen [a], Fungisai Matemadombo [a], Mahmut Durmuş [b], Tebello Nyokong [a,*]

[a] Chemistry of Department, Rhodes University, P.O. Box 94, Grahamstown 6140, South Africa
[b] Gebze Institute of Technology, Department of Chemistry, P.O. Box: 141, 41400 Gebze-Kocaeli, Turkey

ARTICLE INFO

Article history:
Received 25 May 2010
Received in revised form
1 September 2010
Accepted 3 September 2010
Available online 25 October 2010

Keywords:
Octaarylthio-substituted phthalocyanine
Manganese
Water-soluble
Quaternization
Spectroelectrochemistry

ABSTRACT

This paper reports on the synthesis and characterization of new manganese phthalocyanine (MnPc) complexes: 2,3-*octakis*-[(2-mercaptopyridine) phthalocyaninato] acetato manganese (III) (**1**) and its quaternized (hence water soluble) derivative: 2,3-*octakis*-{[(*N*-methyl-2-mercaptopyridine) phthalocyaninato] acetato manganese (III)} sulphate (**2**). The complexes were used to form self assembled monolayers (SAMs). Voltammetry proved that both of the SAMs are well packed, strongly passivating and act as selective and efficient barriers to ion permeability. Furthermore, surface coverage studies confirmed that the MPc macrocycles adsorb onto the gold electrode as monolayers. Both MPc SAMs were successfully used as electrochemical sensors of nitrite.

1. Introduction

Metallophthalocyanines (MPcs) are macrocyclic π-electron conjugated molecules which exhibit a series of electrochemical processes and can consequently be used as efficient electron mediators, for example, in electrocatalysis [1–6].

The presence of electron donating sulfur groups will result in the shift of the Q-band to longer wavelengths compared to unsubstituted MPc. Pc complexes containing Mn as a central metal, in particular, show a highly red-shifted Q-band [7]. The presence of sulfur will also make oxidation of these complexes favourable. Hence, in this work, we present the synthesis and electrochemistry of new sulphur substituted MnPc complexes (**1** and **2**, Scheme 1) and we compare their electrochemical behaviour with those of tetrasubstituted counterparts: manganese (III) 2,(3)-*tetra*-(2-mercaptopyridine) phthalocyanine (β-(OH)MnTMPyPc, **3β**) and its quaternized derivative manganese (III) 2,(3)-*tetra*-*N*-methyl{(2-mercaptopyridine) phthalocyanine (β-(OH)Mn-Q-TMPyPc, **4β**)}, Fig. 1. The syntheses and characterization of complexes **3** and **4** have been previously reported [8]. The water solubility of MnPc complexes is desirable despite the fact that the aggregation tendency in such a polar medium is very high. Hence, we present here the synthesis of a water soluble octa-substituted MnPc derivative (**2**).

MnPc complexes show interesting electrochemical behaviour with oxidation states of the central Mn ion ranging from Mn^{I} to Mn^{IV} [8–15]. The spectra of $Mn^{II}Pc$ and $Mn^{III}Pc$ complexes are now well known. For MnPc complexes tetra substituted with 2-mercaptopyridine at the peripheral positions (**3β**) and then quaternized to give **4β**, spectroelectrochemistry showed that the reduction of $Mn^{II}Pc$ to $Mn^{I}Pc$ occurs only when the complex is in its quaternized form (**4β**). The reduction (to $Mn^{I}Pc^{-2}$) of the quaternized form occurs at a lower potential than that of the unquaternized form (to $Mn^{II}Pc^{-3}$), showing that metal (to $Mn^{I}Pc^{-2}$) versus ligand reduction (to $Mn^{II}Pc^{-3}$) in $Mn^{II}Pc$ complexes may depend on the nature of the ring substituents. This work explores the effect of increasing the number of substituents on the electrochemical behaviour of the mercaptopyridine substituted MnPc derivatives. Furthermore, arylthio derivatised MnPcs in this work are attached to gold electrodes to form self-assembled monolayers (SAMs). Alkyl or arylthio MPcs are known to form SAMs without cleavage of the aryl or alkyl group [16]. The SAMs are employed for the analyses of nitrite.

2. Experimental

2.1. Materials

Acetone was provided by Protea Chemicals and distilled before use. Dimethylformamide (DMF), methanol (MeOH), *n*-pentanol,

* Corresponding author. Tel.: +27 46 6038260; fax: +27 46 6225109.
E-mail address: t.nyokong@ru.ac.za (T. Nyokong).

0143-7208/$ – see front matter © 2010 Elsevier Ltd. All rights reserved.
doi:10.1016/j.dyepig.2010.09.012

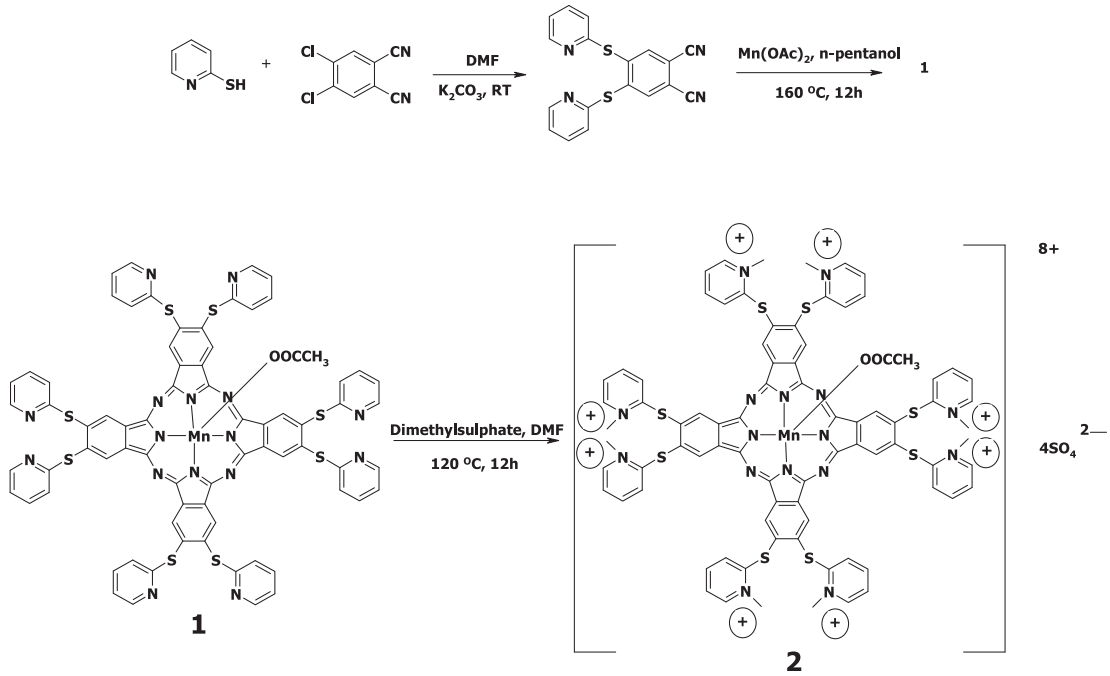

Scheme 1. Synthesis route of 2-mercaptopyridine substituted manganese (III) phthalocyanine complexes (**1** and **2**).

n-hexane, tetrahydrofuran (THF), chloroform, dichloromethane (DCM), ethanol, ethyl acetate, nitric acid (55%), H_2SO_4, buffer (pH 4 and 7) tablets were procured from Saarchem. Deionised water was obtained from a Millipore-Q system. Nitrogen gas was purchased from Afrox. Manganese (II) acetate, K_2CO_3, dimethylsulphate (DMS), tetrabutylammonium tetrafluoroborate ($TBABF_4$) and 1,8-diazabicyclo-[5.4.0]-undec-7-ene (DBU) were purchased from Aldrich. 2-Mercaptopyridine was purchased from Fluka. 4,5-Dichlorophthalonitrile was synthesized and purified according to the literature procedure [17]. All solvents were dried as described by Perrin and Armarego [18] before use. All other reagents were obtained from commercial suppliers and used as received. Sodium nitrite was purchased from Merck. Column chromatography was performed on silica gel 60 (Merck, 0.04–0.063 mm).

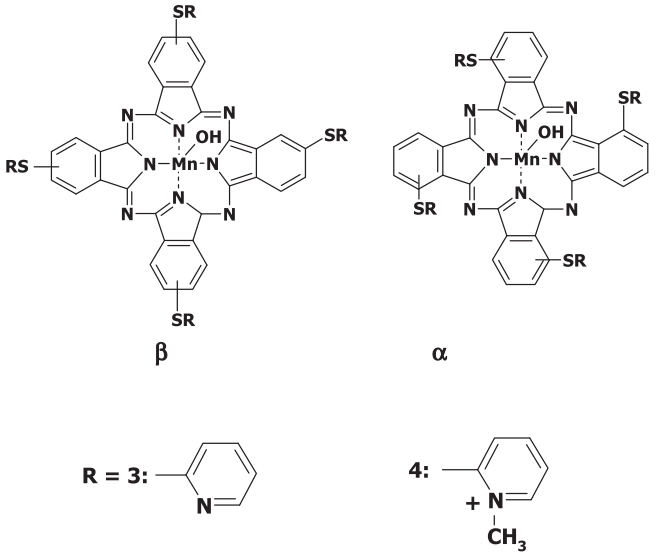

Fig. 1. Molecular structure of tetra substituted complexes **3** and **4**. **3β** and **4β** are peripherally substituted as shown in this figure. **3α** and **4α** are non-peripherally substituted [8].

2.2. Equipment

All electrochemical experiments were performed using Autolab potentiostat PGSTAT 302 (Eco Chemie, Utrecht, The Netherlands) driven by the general purpose Electrochemical data processing software (GPES, software version 4.9). Square wave voltammetric analysis was carried out at a frequency of 10 Hz, amplitude: 50 mV and step potential: 5 mV. A conventional three electrode system consisting of a glassy carbon working electrode (1.5 mm radius), Ag|AgCl pseudo reference electrode and a platinum wire counter electrode were employed. The potential response of Ag|AgCl pseudo reference electrode was less than the Ag|AgCl (3M KCl) by 0.015 ± 0.003 V. All electrochemical experiments were performed at 25.0 ± 1.0 °C using freshly distilled solvents.

UV-visible spectra were recorded on a Shimadzu 2001 UV–Vis spectrophotometer or on a Cary 500 UV-visible/NIR spectrophotometer. Spectroelectrochemical data were recorded using an optically transparent thin-layer electrochemical (OTTLE) cell connected to a BioAnalytical System (BAS) 27 voltammogram. FT-IR spectra (KBr pellets) were recorded on a Bio-Rad FTS 175C FTIR spectrometer. The mass spectra were acquired on a Bruker Daltonics (Bremen, Germany) MicrOTOF mass spectrometer equipped with an electronspray ionization (ESI) source. The instrument was operated in positive ion mode using a *m/z* range of 50–3000. The capillary voltage of the ion source was set at 6000 V and the capillary exit at 190 V. The nebulizer gas flow was 1 bar and drying gas flow 8 mL/min. The drying temperature was set at 200 °C for synthesized phthalonitrile compound and positive ion and linear mode MALDI-MS spectrum of phthalocyanine complexes was obtained in 3,5-dimethoxy-4-hydroxycinnamic acid MALDI matrix using nitrogen laser accumulating 50 laser shots using a Bruker Microflex LT MALDI-TOF mass spectrometer. ^1H spectra were recorded in $CDCl_3$ solution for phthalonitrile compound on a Varian 500 MHz spectrometer. Elemental analyses were obtained with a Thermo Finnigan Flash 1112 Instrument.

2.3. Syntheses

2.3.1. Synthesis of 4,5-bis(2-mercaptopyridine)phthalonitrile, Scheme 1

In a stream of nitrogen, 2-mercaptopyridine (6.74 g, 60.8 mmol) and 4,5-dichlorophthalonitrile (6.00 g, 30.4 mmol) were dissolved in DMF (100 mL) and the mixture stirred at room temperature for 30 min. Thereafter, finely ground K_2CO_3 (15 g, 108 mmol) was added portion-wise over a period of 4 h and the reaction mixture left to stir for a further 12 h at room temperature. The mixture was added to water (200 mL) and stirred for 30 min. The resulting precipitate was filtered off, thoroughly washed with water, dried and recrystallised from chloroform:ethanol (1:4). M.p.: 220 °C Yield: 5.79 g (55%). IR [(KBr) ν_{max}/cm^{-1}]: 3037 (Ar-CH), 2230 (C≡N), 1574 (C=C). ^{1}H-NMR ($CDCl_3$): δ, ppm 8.55 (d, 2H, Pyridyl-H), 7.83 (s, 2H, Phthalonitrile-H), 7.70 (t, 2H, Pyridyl-H), 7.38 (d, 2H, Pyridyl-H), 7.28 (t, 2H, Pyridyl-H). Calc. for $C_{18}H_{10}N_4S_2$: C 62.41, H 2.91, N 16.17; Found: C 62.20, H 2.80, N 16.17. MS (ESI-MS) *m/z*: Calc. 346; Found: 347.1 $[M+H]^+$.

2.3.2. 2,3-Octakis(2-mercaptopyridine)phthalocyaninato manganese (III) acetate (**1**, Scheme 1)

A mixture of anhydrous manganese (II) acetate (0.50 g, 2.88 mmol), 4,5-*bis*(2-mercaptopyridine)phthalonitrile (1.0 g, 2.88 mmol), DBU (0.44 mL, 3 mmol) and *n*-pentanol (25 mL) was stirred at 160 °C for 12 h under nitrogen atmosphere. After cooling, the solution was dropped into *n*-hexane. The brown solid product was precipitated and collected by filtration and washed with *n*-hexane. The crude product was washed with water, ethanol, acetone, THF, $CHCl_3$, *n*-hexane and diethyl ether. The brown crude product was purified by passing through a silica gel column with firstly ethyl acetate and then CH_2Cl_2:MeOH (10:1) elution. Yield: 0.63 g (59 %). UV–Vis (DMF): λ_{max} nm (log ϵ) 355 (4.49), 586 (3.86), 647 (4.75), 703 (4.00). IR [(KBr) ν_{max}/cm^{-1}]: 3041 (Ar-CH), 1724 (C=O), 1571(C=C), 1556, 1445, 1415, 1321, 1278, 1119, 1070, 984, 956, 895, 755. Calc. for $C_{74}H_{43}N_{16}S_8O_2Mn$: C 59.27, H 2.89, N 14.94; Found: C 59.61, H 2.96, N 14.34. MALDI-TOF-MS *m/z*: Calc. 1498; Found: 1439.7 $[M\text{-}COOCH_3]^+$.

2.3.3. 2,3-Octakis[(N-methyl-2-mercaptopyridine) phthalocyaninato manganese (III) acetate] sulphate (**2**, Scheme 1)

Compound **1** (0.20 g, 0.13 mmol) was heated to 120 °C in freshly distilled DMF (10 mL) and dimethyl sulphate (0.2 mL) was added dropwise. The mixture was stirred at 120 °C for 12 h, cooled to room temperature and the product was precipitated with hot acetone and collected by filtration. The greenish brown solid product was washed successively with hot ethanol, ethyl acetate, THF, chloroform, *n*-hexane and diethylether. The resulting hygroscopic product was dried over phosphorous pentoxide. Yield: 0.21 g (79 %). UV–Vis (H_2O): λ_{max} nm (log ϵ) 376 (4.54), 577 (3.92), 625 (4.27), 697 (5.08). IR [(KBr) ν_{max}/cm^{-1}]: 3047 (Ar-CH), 2951 (CH), 1732 (C=O), 1567 (C=C), 1490, 1216 (S=O), 1161 (S=O), 1056, 1043, 846, 765, 741, 618 (S–O). Calc. for $C_{82}H_{73}N_{16}O_{21}S_{12}Mn$ ($3H_2O$): C 47.85, H 3.57, N 10.89; Found: C 48.12, H 3.96, N 10.29. MALDI-TOF-MS *m/z*: Calc. 2004.2; Found 1891.3 $[M\text{-}COOCH_3\text{-}Mn]^+$.

2.4. The preparations of SAMs

The gold electrode was cleaned by immersing it for approximately 2 minutes in a hot solution of 1:3 (v:v) nitric acid (55%) and concentrated H_2SO_4. This procedure removes organic impurities on the electrode. This was then followed by polishing the gold electrode, using aqueous slurries of alumina (<10 micron), on a SiC-emery paper (type 2400 grit), and then to a mirror finish on a Buehler-felt pad. Finally the Au electrode was rinsed in copious amounts of ultrapure Millipore water and acetone to remove residual alumina particles trapped at the surface.

This pre-treatment was followed by placing the Au electrode in a DMF solution of 1 mM of solutions of complexes **1** or **2** for 24 h at room temperature to form the SAM. Upon removal from the MnPc solution, the electrode was rinsed with buffer before any electrochemical analysis.

3. Results and discussion

3.1. Syntheses and characterization

The metallophthalocyanine complex (**1**) was prepared by the template reaction of thiol-substituted phthalonitrile precursor with anhydrous manganese (II) acetate in the presence of DBU using *n*-pentanol as solvent. Column chromatography with silica gel was employed to obtain the pure products from the reaction mixture resulting in a 59 % yield for complex **1**. Quaternization of the manganese (III) phthalocyanine compound was achieved at 120 °C. Yield of the product was 79 % for complex **2**.

Generally, phthalocyanine compounds are insoluble in most organic solvents; however, introduction of substituents on the ring increases the solubility. The quaternized manganese (III) phthalocyanine complex (**2**) exhibited excellent solubility in water. The new compounds were characterized by UV-vis, IR and NMR spectroscopies (the latter for the phthalonitrile only), ESI-MS (for the phthalonitrile compound), MALDI-TOF mass spectra and elemental analysis. The analyses are consistent with the predicted structures as shown in the experimental section. The sharp peak in the IR spectra for the C≡N vibrations of phthalonitrile at 2230 cm^{-1} disappeared after conversion into manganese (III) phthalocyanine complex, indicative of metallophthalocyanine formation. The characteristic vibrations corresponding to C=C groups at ~1570 cm^{-1}, aromatic CH stretching at 3037–3047 cm^{-1} were observed for all compounds. Aliphatic CH stretches were observed at ~2951 cm^{-1} for quaternized phthalocyanine complex. S=O stretching at ~1216 and ~1161 cm^{-1} and S–O stretching at 618 cm^{-1} for the quaternized phthalocyanine complex (**2**) is indicative of quaternization.

In addition to the elemental analysis results, the mass spectra data for the newly synthesized phthalonitrile and manganese (III) phthalocyanine complexes (**1** and **2**) were consistent with the assigned formulations. The molecular ion peak of phthalonitrile was observed at *m/z* 347.1$[M+H]^+$. The molecular ion peak of the non-quaternized phthalocyanine complex (**1**) was found at *m/z* 1439.7 $[M\text{-}COOCH_3]^+$. The molecular ion peaks of quaternized phthalocyanine complex (**2**) showing parent ions was found at *m/z* 1891.3 $[M\text{-}COOCH_3\text{-}Mn]^+$. MALDI-TOF-MS spectra of quaternized phthalocyanine complex (**2**) show the base peak cleavage of axial ligand and manganese atom. We did not observe the molecular ion peak for quaternized complex **2**.

3.2. UV–Visible spectra

Complex **1** readily dissolves in most organic solvents but is moderately soluble in DCM. Complex **2** did not dissolve in THF, $CHCl_3$, DCM, toluene, acetone (or their combinations) and dissolved with great difficulty in DMF and DMSO (complex **2** should be left overnight in these solutions to dissolve completely). Fig. 2(a) and (b) shows the spectra of complexes **1** and **2** in various solvents, respectively.

It has been suggested [19,20] that an equilibrium exists between MnPc species in DMF under air as shown by equations (1)–(5).

$$PcMn^{\mathbf{II}} + O_2 \rightleftarrows PcMn^{\mathbf{III}}(O_2) \quad (1)$$

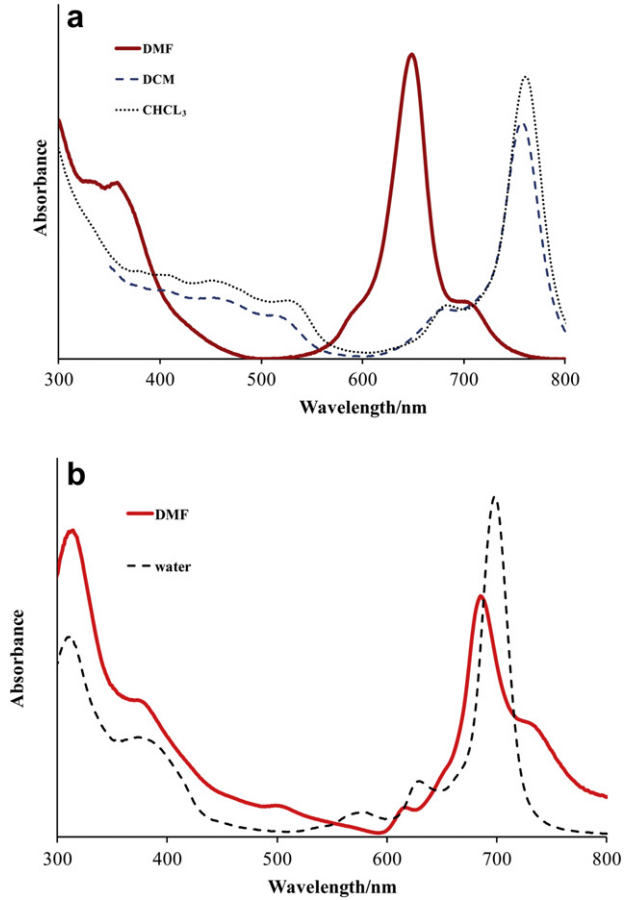

Fig. 2. UV-visible spectra of: (a) **1** in DMF, DCM and $CHCl_3$ and (b) **2** in DMF and H_2O.

$$PcMn^{III}(O_2) + PcMn^{II} \rightleftarrows PcMn^{III}\text{-}O_2\text{-}Mn^{III}Pc \quad (2)$$

$$PcMn^{III}\text{-}O_2\text{-}Mn^{III}Pc \rightleftarrows 2PcMn^{IV}O \quad (3)$$

$$2PcMn^{IV}O + 2PcMn^{II} \rightleftarrows 2PcMn^{III}\text{-}O\text{-}Mn^{III}Pc \quad (4)$$

$$4PcMn^{II} + O_2 \rightleftarrows 2PcMn^{III}\text{-}O\text{-}Mn^{III}Pc \text{ (Net equation)} \quad (5)$$

Thus, in general, the electronic absorption spectra in the visible region for MnPc complexes may be attributed to $Mn^{III}Pc$, $Mn^{II}Pc$ and μ-oxo MnPc species in DMF under air. The presence of the μ-oxo MnPc species may be confirmed by monitoring the spectral transformations of an MPc complex DMF solution when not de-aerated and when de-aerated with dry N_2 gas; this was done in this work. Thus in Fig. 2a (complex **1**), the spectra in DMF is mainly that of the μ-oxo MnPc species with a strong band at 651 nm [15,21] and the $Mn^{II}Pc$ peak at 708 nm. The $Mn^{III}Pc$ peak is not evident in Fig. 2a. This peak would have been expected to be red shifted as observed in the other solvents in Fig. 2a. The intensity of the 651 nm band (due to μ-oxo MnPc species) decreased on bubbling argon through the solution and there was an increase in the intensity of the band at 708 nm due to $Mn^{II}Pc$ species. The spectra of complex **1** in chloroform and DCM is typical of Mn(III)Pc species, showing a red shifted Q band.

Complex **2** in DMF (Fig. 2b) showed the $Mn^{II}Pc$ absorption band at 688 nm, $Mn^{III}Pc$ as a broad peak near 730 nm, the peak due to μ-oxo MnPc species was not well defined, showing that the quaternized derivative (**2**) has a less tendency of forming μ-oxo complexes than complex **1**. In water, complex **2** showed no presence of μ-oxo complexes. The spectrum of the quaternized complex **2** were blue shifted compared to the corresponding MnPc species of unquaternized derivative (**1**), Fig. 2. This is due to the lowering of the electron donating ability of the nitrogen groups upon quaternization.

3.3. Voltammetric and spectroelectrochemical studies

3.3.1. 2,3-Octakis-[(2-mercaptopyridine) phthalocyaninato] acetato manganese (III) (**1**)

Solution redox properties of **1** were studied using cyclic voltammetry (CV) and square wave voltammetry (SWV) in freshly distilled DMF. Argon was bubbled through the solution and an argon atmosphere was maintained throughout the cyclic voltammetry scans, hence the species being analysed is not expected to contain μ-oxo species, though its presence cannot be completely ruled out.

Three redox processes (**I**–**III**) were observed for complex **1** in DMF, Fig. 3a. All processes were reversible to quasi-reversible with cathodic to anodic peak potential (ΔE) ranging from 60 to 100 mV (the ΔE for the ferrocene standard was 65 mV). In comparison with literature [8,22], Table 1, processes **III** and **II** for complex **1** in DMF (Fig. 3a) are assigned to $Mn^{III}Pc^{-2}/Mn^{II}Pc^{-2}$ ($E_{1/2} = 0.023$ V) and $Mn^{II}Pc^{-3}/Mn^{II}Pc^{-2}$ ($E_{1/2} = -0.69$ V), respectively. Process **I** ($E_{1/2} = -1.09$ V) is then assigned as a further ring reduction process. Comparing complexes **1** and **3β** (structure shown in Fig. 1), confirms that process **II** is ring based $Mn^{II}Pc^{-2}/Mn^{II}Pc^{-3}$ rather than metal based $Mn^{II}Pc^{-2}/Mn^{I}Pc^{-2}$. The observed broadening of redox couple **II** is ascribed to the aggregation as a result of the high concentrations (1×10^{-3} M) used for voltammetry analysis. This is affirmed by the square wave voltammogram showing a split redox couple **II** where one is due to the monomer and other to the aggregate [23]. Table 1 shows that complex **1** is easier to reduce than the corresponding complexes **3α** and **3β**. The presence of electron donating sulphur groups is expected to make oxidation easier and reduction more difficult. However when comparing with other MnPc complexes such as manganese tetraamino phthalocyanine derivatives (with Mn^{III}/Mn^{II} process occurring at ~ −0.3 V vs Ag|AgCl for the same electrolyte/solvent system) [24], complex **1** is easier to reduce.

3.3.2. 2,3-Octakis-{[(N-methyl-2-mercaptopyridine) phthalocyaninato] acetato manganese (III)} sulphate (**2**)

Fig. 3b shows that three redox processes (labeled **I**–**III**) recorded in DMF containing $TBABF_4$ were obtained for complex **2**. Couple **II** shows splitting due to aggregation. The redox couples **III** and **II** are assigned to $Mn^{III}Pc^{-2}/Mn^{II}Pc^{-2}$ ($E_{1/2} = -0.038$ V) and $Mn^{II}Pc^{-2}/Mn^{I}Pc^{-2}$ ($E_{1/2} = -0.38$ V) in comparison with the corresponding tetrasubstituted derivatives, Table 1. Couple **I** ($E_{1/2} = -0.64$ V) is assigned to ring based reduction, Table 1. Complex **2** is easier to reduce than complexes **4α** and **4β**, which are tetra substituted at different positions. All complexes contain sulphur groups, which are electron donating and expected to result in a more difficult reduction. It would be expected that complex **2** would be more difficult to reduce than both **4α** and **4β** due to the former having more sulphur groups, however, the presence and plurality of positive charges will affect the ease of reduction. In aqueous media the couples were observed at $E_{1/2} = -0.52$ V (ring reduction), $E_{1/2} = -0.41$ V ($Mn^{II}Pc^{-2}/Mn^{I}Pc^{-2}$), $E_{1/2} = 0.053$ V ($Mn^{III}Pc^{-2}/Mn^{II}Pc^{-2}$). Comparison in Table 1 with literature shows that the quaternized derivative (**2**) exhibits the $Mn^{II}Pc^{-2}/Mn^{I}Pc^{-2}$ couple, while the unquaternized derivative (**1**) shows the $Mn^{II}Pc^{-2}/Mn^{II}Pc^{-3}$ couple [8].

3.3.3. Spectroelectrochemical studies

Fig. 4 shows the application of potentials more negative than couple **III** for complex **2** in DMF. The spectrum before electrolysis in

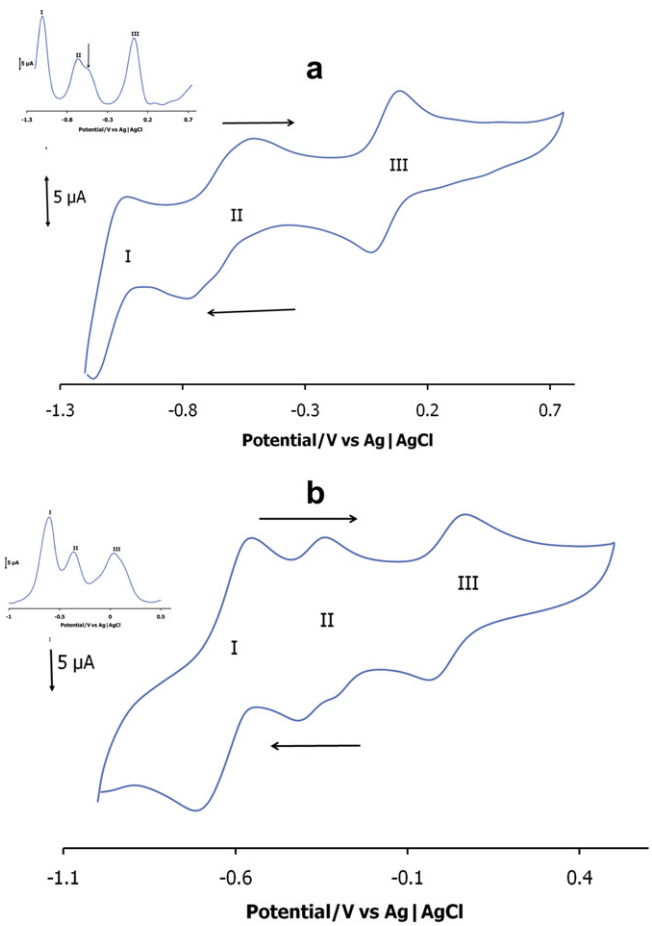

Fig. 3. Cyclic and square wave (insert) voltammograms on a GCE recorded in DMF containing 0.1 M $TBABF_4$ for (a) **1** and (b) **2**. Scan rate = 100 mV s^{-1}. The arrow in insert for (a) shows the peak due to the aggregate.

DMF shows monomeric behaviour and the presence of mainly $Mn^{III}Pc$ species, when compared to Fig. 2b. This again shows the strong effects of the presence of oxygen in solution. Solutions for spectroelectrochemistry were extensively deaerated, but the presence of μ-oxo MnPc cannot be completely ruled out as stated above. Upon reduction at potentials of couple **III**, a blue shift in the Q-band was observed from 729 nm to a weak peak at ~ 685 nm which is typical of Mn^{III} reduction to Mn^{II} [15], and a stronger μ-oxo MnPc peak was observed at 648 nm. The μ-oxo MnPc would be a result of the presence of residual oxygen in solution, even after deoxygenating with argon. Concurrently, a charge transfer band at 541 nm also increased in intensity. Upon regeneration of the Mn^{III} species, only 60 % could be obtained which is ascribed to the reduction of Mn^{II} concentration by molecular oxygen. These spectral observations thus confirmed the assignment of redox couple **III** to the metal reduction process $Mn^{III}Pc^{-2}/Mn^{II}Pc^{-2}$. Due to the presence of the μ-oxo MnPc species further reduction (at process **II**) was not possible. Spectral changes similar to those observed in DMF were also observed in water upon reduction of **2** at potentials of process **III**.

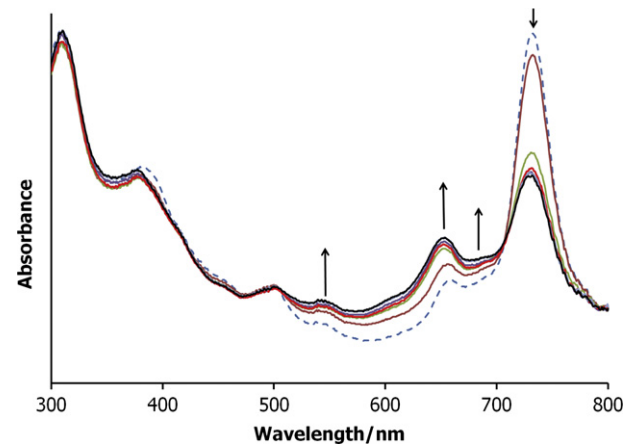

Fig 4. UV-visible spectral changes of **2** in DMF containing 0.1 M $TBABF_4$ upon reduction at potentials of process **III** (~−0.3 V).

3.4. Self assembled monolayer (SAM) characterization

Voltammetry techniques for the characterization of SAMs are based on the principle that SAMs block a number of Faradic processes [25].

3.4.1. Ion barrier factor (Γ_{ibf})

The ion barrier factor (Γ_{ibf}) is obtained by comparison of the total charge under the gold redox peak of a SAM modified electrode (Q_{SAM}) with that of an un-modified electrode (Q_{Bare}), Eq. (6):

$$\Gamma_{ibf} = 1 - \frac{Q_{SAM}}{Q_{Bare}} \quad (6)$$

An ion barrier factor of one indicates that there are no pinholes in the SAM and that it is an ideal barrier to ion and solvent permeability [25,26].

Fig. 5(a) shows the cyclic voltammograms of SAMs of complexes **1** and **2** (labeled 1 and 2 respectively) and unmodified gold electrode (labeled 3) recorded in 1 M Na_2SO_4 in pH 4 buffer solution.

Table 1
Redox potentials (V vs. Ag|AgCl) for MnPc derivatives.

Complex[a]	Solvent/Electrolyte[c]	$Mn^{II}Pc^{-3}/Mn^{II}Pc^{-4}$	$Mn^{II}Pc^{-2}/Mn^{II}Pc^{-3}$	$Mn^{II}Pc^{-2}/Mn^{I}Pc^{-2}$	$Mn^{III}Pc^{-2}/Mn^{II}Pc^{-2}$	Ref.
1	DMF/$TBABF_4$	−1.15	−0.69 −0.60[b]		0.023	This work
β-(OH)MnTMPyPc (**3β**)	DMF/$TBABF_4$		−0.71		−0.057	8
2	DMF/$TBABF_4$		−0.64[c]	−0.31(E_p)[b] −0.38	−0.038	This work
2	H_2O/TBAP[d]		−0.52[c]	−0.41	0.053	This work
β-(OH)Mn-Q-TMPyPc (**4β**)	DMF/$TBABF_4$			−0.56	−0.063	8
α-(OH)MnTMPyPc (**3α**)	DMF/$TBABF_4$		−0.76		−0.051	8
α-(OH)Mn-Q-TMPyPc (**4α**)	DMF/$TBABF_4$			−0.59	−0.056	8

[a] TMPyPc = *tetra*-(2-mercaptopyridine)phthalocyanine, Q-TMPyPc = quaternized *tetra*-(2-mercaptopyridine)phthalocyanine; β = peripheral substitution, α = non-peripheral substitution.
[b] Shoulder.
[c] Tentatively assigned to $Mn^{I}Pc^{-2}$ /$Mn^{I}Pc^{-3}$.
[d] TBAP = tetrabutyl ammonium perchlorate.

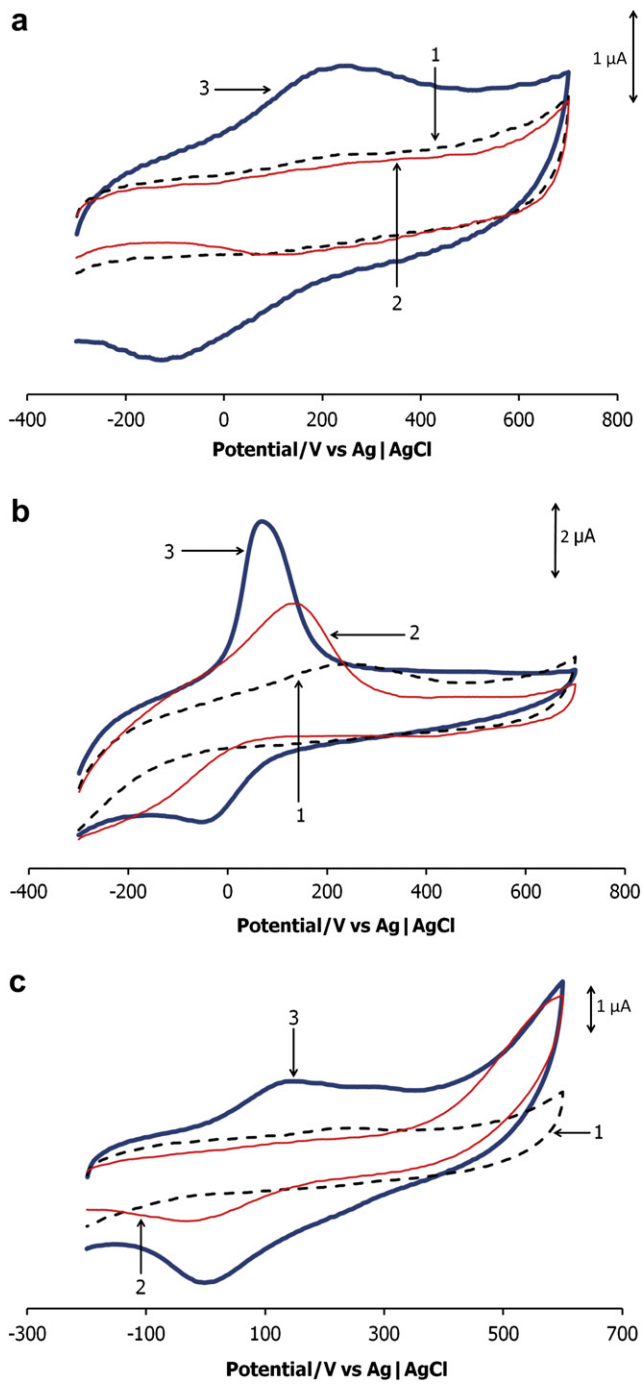

Fig. 5. Cyclic voltammograms (1st scans) of SAM complexes **1** and **2** (labeled 1 and 2 respectively) and unmodified gold electrode (labeled 3) recorded in: (a) 1 M Na_2SO_4 in pH 4 buffer solution; (b) 1 mM $CuSO_4$ in pH 4 buffer solution (c) 1 mM Fe $(NH_4)_2(SO_4)_2 \cdot 6H_2O$ in 1 M $HClO_4$ solution. Scan rate = 100 mV s^{-1}.

The peaks observed on the un-modified gold electrode (curve 3) are due to the gold oxide redox reaction. Upon modification, the peaks disappear completely for both the complexes (curves 1 and 2). From Fig. 5(a), ion barrier factors of 0.9955 and 0.9952 for **1** and **2** respectively were obtained (using Eq. (6)), Table 2. These results show that only ~1 % of the gold surface is not covered by the complex SAMs and that the SAMs are compact and virtually defect free. Furthermore, the obtained values compare favourably to those of similarly structured molecules that have recently been published in the literature [27,28].

3.4.2. Interfacial capacitance (C_s)

A defined potential window of a cyclic voltammogram, in which no peaks are observed for both unmodified and SAM modified gold electrodes, will have a charging current (i_{ch}), whose value may be used to calculate the interfacial capacitance (C_s) using Eq. (7):

$$C_s = \frac{i_{ch}}{\nu A} \tag{7}$$

where ν is the scan rate (V s^{-1}) and A is the electrode surface area (cm^2).

The lower the C_s value, the fewer are the defects present in the SAM and so the less permeable is the electrode surface to electrolyte ions [26,29]. A SAM modified gold electrode should therefore display a lower C_s value than an unmodified gold electrode.

Fig. 5(a) was used to estimate the C_s values which were found to be of 391 and 577 μF cm^{-2} for **1** and **2** respectively (using Eq. (7)), Table 2. The C_s values are lower than for an un-modified gold electrode (C_s = 1500 μF cm^{-2}). The decrease in C_s on formation of SAMs is attributed to closely packed, relatively defect free SAM layers.

3.4.3. Underpotential deposition (UPD) of copper

Fig. 5(b) shows how the SAMs of complexes **1** and **2** (curve 1 and 2 respectively) inhibit the Faradic process of Cu metal deposition onto a gold electrode relative to an unmodified gold electrode (curve 3). The bulk deposition of copper began at approximately +0.1 V vs. Ag|AgCl during the negative going scan of the un-modified gold electrode, Fig. 5(b). A large underpotential deposition (UPD) stripping peak for the Cu metal is observed between 0 and 0.15 V on the return scan (Fig. 5(b), curve 3). This peak has a characteristic shape and occurs in a similar potential window to that previously published [29,30]. Negligible current responses are observed on the cyclic voltammogram of complex **1** SAM (curve 1) relative to that of the un-modified gold electrode (curve 3), Fig. 5(b). Lower intensity peaks were observed for **1** relative to **2**, Fig. 5(b). Therefore, from Fig. 5(b), the SAM of **1** covers the gold surface better than **2** because the gold surface is no longer fully accessible to the Cu solution and hence the redox reaction is not clearly observed for **1**. Complex **2** is less effective in covering the gold electrode.

3.4.4. Inhibition of Fe^{III}/Fe^{II} redox processes

Fig. 5(c) shows the cyclic voltammograms of an unmodified gold electrode (curve 3) and gold electrodes modified with **1** and **2** SAMs (curves **1** and **2** respectively) recorded in $[Fe(H_2O)_6]^{3+}/[Fe(H_2O)_6]^{2+}$ in 1 M $HClO_4$ solution. $Fe(NH_4)SO_4$ in $HClO_4$ was used as the analyzing electrolyte because its redox couple $[Fe(H_2O)_6]^{3+}/[Fe(H_2O)_6]^{2+}$ has a lower electron transfer rate constant than [Fe

Table 2
Characterization parameters of SAMs.

Parameter	1	2	3β	4β	3α	4α
Ion Barrier Factor, Γ_{ibf}	0.9955	0.9952	0.9997	0.9994	0.9998	0.9996
Interfacial Capacitance, C_s (μF cm^{-2})	391	577	452	539	303	302
Surface Coverage, Γ (mol cm^{-2})	2.40×10^{-10}	1.14×10^{-10}	1.73×10^{-10}	2.77×10^{-10}	2.80×10^{-10}	2.67×10^{-10}

$(CN)_6]^{3-}/[Fe(CN)_6]^{4-}$ and hence mass transport does not determine the reaction rate, even at small overpotentials [31]. The Faradic couple $[Fe(H_2O)_6]^{3+}/[Fe(H_2O)_6]^{2+}$ occurring in Fig. 5(c) in the −0.1 to +0.4 V region on the un-modified gold electrode (curve 3) is largely inhibited for both of the SAM modified gold electrodes. Complex **1** (curve 1) SAM displayed the best inhibition of the redox processes showing that this film is more compact and acts as better barrier to the transport of $[Fe(H_2O)_6]^{3+}/[Fe(H_2O)_6]^{2+}$ ions relative to **2**.

3.4.5. Surface coverage (Γ)

A linear plot of background corrected peak current vs. the scan rate for the peaks of adsorbed SAM were obtained (not shown) and was used to calculate surface coverage (Γ) using Eq. (8) [25]:

$$i_p = \frac{n^2F^2A\Gamma(\upsilon)}{4RT} \quad (8)$$

where i_p is the peak current (amps), n is the number of electrons, F is the Faraday constant ($F = 96{,}485\ C\ mol^{-1}$), A is the real surface area of the electrode (0.021 cm^2), ν is the scan rate ($V\ s^{-1}$), R is the gas constant ($R = 8.314\ J\ K^{-1}\ mol^{-1}$), and T is the temperature in Kelvin. The Γ values of the MnPc SAMs, Table 2, are 2.40×10^{-10} and 1.14×10^{-10} mol cm^{-2} for **1** and **2** respectively. The Γ value for **2** the value is within the range (1×10^{-10} mol cm^{-2}) reported for adsorbed monolayers of other metallophthalocyanines lying flat on the electrode [32–34]. The value for **1** is higher than reported for molecules lying flat on the electrode, hence may suggest a different orientation on the electrode. This also applies to complexes **3β**, **4β**, **3α** and **4α** in Table 2.

3.5. Detection of nitrite on SAMs

Nitrite was employed in this work to probe the effectiveness of SAMs in electrocatalysis. Fig. 6 shows the cyclic voltammograms of unmodified (curve 1) and SAMs of complexes **1** (curve 2) and **2** (curve 3) recorded in 1 mM nitrite (in pH 7 buffer solution). The disproportionation of nitrite to NO is insignificant at the pH used, thus the observed responses are for the oxidation of nitrite, not nitric oxide. A weak peak was observed for nitrite on an unmodified gold electrode (Fig. 6, curve 1). Nitrite oxidation peaks were observed at 0.74 V vs. Ag|AgCl for SAMs of the MnPc complexes, Table 3. Nitrite oxidation occurs on the un-modified gold electrode at approximately 0.77 V vs. Ag|AgCl, but the peak current is enhanced upon modification with all of the SAMs. The values of the nitrite detection potentials for the MnPc SAMs compare well with the literature, Table 3 [27,35,36].

Table 3
Electrochemical parameters for nitrite determination.

MPc	LOD (M)	E_p (V) *vs.* Ag|AgCl	Tafel Slope (mV $decade^{-1}$)	α	n_t	Sensitivity ($A\ M^{-1}\ cm^{-2}$)	Ref.
1	2.94×10^{-7}	0.74	134	0.56	1.78	0.28	This work
2	1.97×10^{-7}	0.74	174	0.66	1.81	0.42	This work
3β	2.69×10^{-7}	0.72	157	0.62	2.06	0.31	27
4β	2.72×10^{-7}	0.74	167	0.65	1.99	0.46	27
3α	3.02×10^{-7}	0.74	152	0.61	2.01	0.27	27
4α	1.78×10^{-7}	0.76	94	0.37	2.00	0.37	27

Linear relationships between the peak current and the square root of the scan rate were obtained for complexes **1** and **2** SAMs indicating diffusion controlled electrocatalytic oxidation of nitrite.

The Tafel slopes were determined using the standard equation (Eq. 9) for a totally irreversible process [37]:

$$E_p = \frac{2.3RT}{2(1-\alpha)nF}\log \upsilon + K \quad (9)$$

where α is the transfer coefficient, ν is the scan rate, n is the number of electrons involved in the rate determining step, and K is a constant. Tafel slopes were obtained from plots of log scan rate versus potential, Fig. 7a (for **1** as an example). Tafel slopes were 134

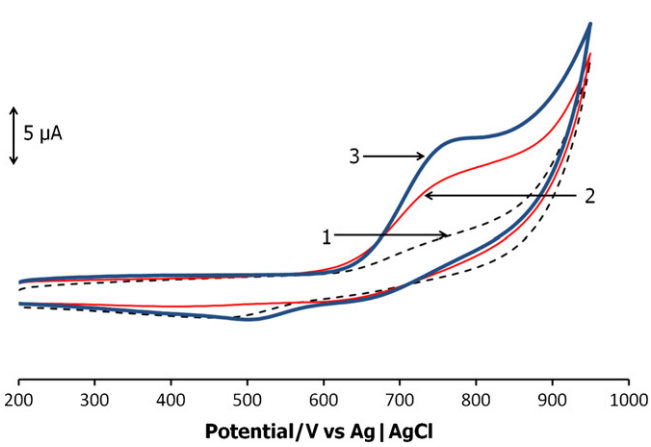

Fig. 6. Cyclic voltammograms of: unmodified Au electrode (1) and SAMs of complexes **1** (2) and **2** (3) recorded in 1 mM nitrite (in pH 7 buffer solution). Scan rate = 100 mV s^{-1}.

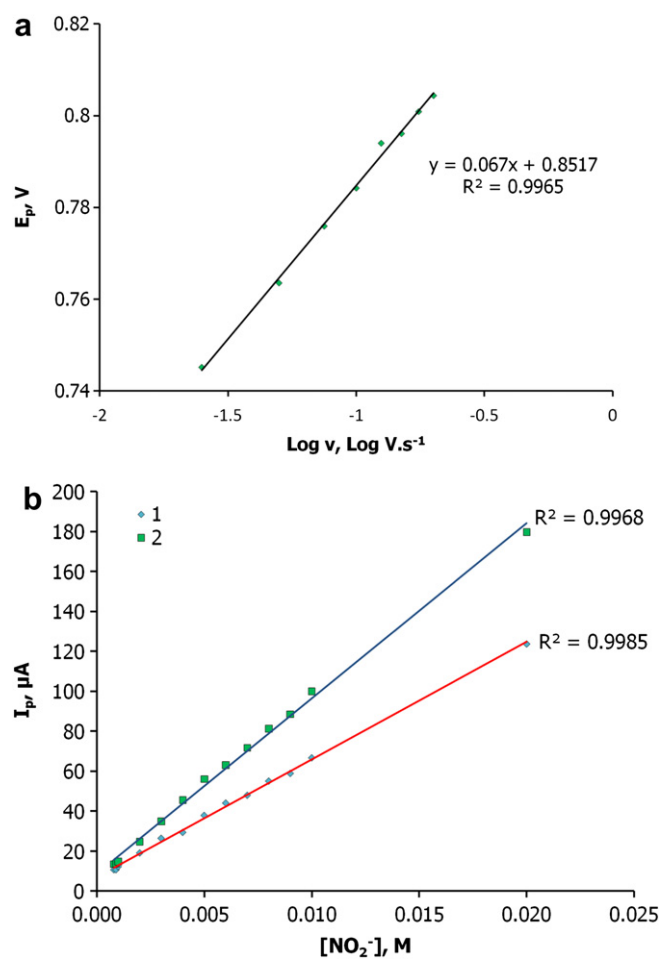

Fig. 7. (a) plot of E_p *vs.* log υ for 1 mM nitrite in pH 7 buffer solution on SAM of complex **1**. (b) Plot of the peak current *vs.* nitrite (in pH 7 buffer solution) concentration for SAMs of complexes **1** and **2**.

and 174 mV decade^{-1} for **1** and **2** respectively, suggesting that the first one electron transfer is rate determining. These values are higher than the normal 30 to 120 values indicating either chemical reactions coupled to electrochemical steps or interaction between nitrite and catalyst [34,38], Table 3.

There is a greater probability of forming products in the reaction transition state by both SAMs of this work because they had α values greater than 0.5, Table 3. Again, since most of the Tafel slopes are large and do not fall within the usual 30 to 120 mV decade^{-1} region, the α values are tentative.

The total number of electrons (n_t) involved in the electrocatalytic oxidation of nitrite by the SAMs was calculated using Eq. (10), valid for a totally irreversible electrode process [37]:

$$i_p = 2.99 \times 10^5 n_t[(1-\alpha)n]^{\frac{1}{2}} A C_o D^{\frac{1}{2}} \upsilon^{\frac{1}{2}} \quad (10)$$

where A is the area of the electrode (cm^2), C_o is the concentration of nitrite (mol cm^{-3}), and D is the diffusion coefficient of nitrite $D = 2.1 \times 10^{-5}$ cm^2 s^{-1} [39,40]). The total number of electrons transferred was calculated to be 1.78 and 1.81 for complexes **1** and **2** SAMs respectively, Table 3. The mechanism with two electrons transferred will be the same as reported before [41].

Fig. 7b shows that there is a linear relationship between the peak current and the nitrite ion concentration (10^{-4}–10^{-2} M range) for the SAMs of this work making the electrodes useful for analyses of nitrite concentrations within the shown range. The sensitiveness of the complexes **1** and **2** SAMs were 0.28 A M^{-1}cm^{-2} and 0.42 A M^{-1}cm^{-2} respectively, Table 3. Detection limits of 2.95×10^{-7} M and 1.97×10^{-7} M (3σ criterion) for complexes **1** and **2** SAMs, respectively, were observed. These values are comparable to those of the corresponding tetrasubstituted derivatives in Table 3. The low detection suggests that the SAMs have good potential for use as nitrite sensors. Both SAMs showed good short term stability as there was less than 10% decay in current output after 35 continuous cyclic voltammetry recordings.

4. Conclusion

MnPc complexes substituted with thio groups (2,3-*octakis*-(2-mercaptopyridine) phthalocyaninato manganese (III) acetate (**1**) and 2,3-*octakis*-[(*N*-methyl-2-mercaptopyridine) phthalocyaninato manganese (III) acetate] sulphate (**2**)) were synthesized and characterized *via* spectroscopic and electrochemical methods. The new complexes were used to form self assembled monolayers (SAMs). Both MPc SAMs were successfully used as electrochemical sensors of nitrite.

Acknowledgements

This work was supported by the Department of Science and Technology (DST) and National Research Foundation (NRF) of South Africa through DST/NRF South African Research Chairs Initiative for Professor of Medicinal Chemistry and Nanotechnology and Rhodes University and Scientific Research Project of Gebze Institute of Technology (BAP-2007-A-01). FM thanks Rhodes University for a graduate bursary.

References

[1] Nyokong T. In: Zagal JH, Bedioui F, Dodelet JP, editors. N_4-macrocyclic metal complexes. United States of America: Springer; 2006.
[2] Ceyhan T, Altindal A, Özkaya AR, Salih B, Bekaroglu O. Synthesis, characterization, and electrocatalytic and electrical properties of novel ball-type four cyclopentyldisilanoxy-POSS bridged metallophthalocyanines. Dalton Transactions; 2009:10318–29.
[3] Koca A, Dincer HA, Gonca E, Gül A. Voltammetric and spectroelectrochemical characterization and electrocatalytic application of metallo phthalocyanines carrying pendant bulky units. Journal of Porphyrins and Phthalocyanines 2009;1(3):669–80.
[4] Ozoemena KI, Stefan-van Staden RI, Nyokong T. Metallophthalocyanine based carbon paste electrodes for the determination of 2′3′-dideoxyinosine. Electroanalysis 2009;21:1651–4.
[5] Koc I, Camur M, Bulut M, Özkaya AR. Electrocatalytic performances of carbon supported metallophthalocyanine and Pt/metallophthalocyanine catalysts towards dioxygen reduction in acidic medium. Catalysis Letters 2009;131:370–80.
[6] Koç I, Ozer M, Ozkaya AR, Bekaroğlu O. Electrocatalytic activity, methanol tolerance and stability of perfluoroalkyl-substituted mononuclear, and ball-type dinuclear cobalt phthalocyanines for oxygen reduction in acidic medium. Dalton Transactions; 2009:6368–76.
[7] Nyokong T, Isago H. The renaissance in optical spectroscopy of phthalocyanines and other tetraazaporphyrins. Journal of Porphyrins and Phthalocyanines 2004;8:1083–90.
[8] Sehlotho N, Durmuş M, Ahsen V, Nyokong T. The synthesis and electrochemical behaviour of water soluble manganese phthalocyanines: anion radical versus Mn(I) species. Inorganic Chemistry Communications 2008;11:479–83.
[9] Zhu J, Gu F, Zhag J. Preparation and photovoltaic properties of near-infrared absorbing manganese(II) phthalocyanine polymer films. Materials Letters 2007;61:1296–8.
[10] Posiuk-Bronikoswska W, Krajewska M, Pfis-Kabulska I. Transformations of manganesetetrasulphophthalocyanine in oxidative conditions. Polyhedron 1998;18:561–70.
[11] Knecht S, Dürr K, Schmid G, Subramanian LR, Hanack M. Synthesis and properties of soluble phthalocyaninatomanganese(III) Complexes. Journal of Porphyrins and Phthalocyanines 1999;3:292–8.
[12] Rittenberg DK, Baarrs-Hibbe L, Böhm A, Miller JS. Manganese(II) octabutoxynaphthalocyanine and its ferrimagnetic electron-transfer salt with TCNE. Journal of Materials Chemistry 2000;10:241–4.
[13] Mbambisa G, Tau P, Antunes E, Nyokong T. Synthesis and electrochemical properties of purple manganese(III) and red titanium(IV) phthalocyanine complexes octa-substituted at non-peripheral positions with pentylthio groups. Polyhedron 2007;26:5355–64.
[14] Leznoff CC, Black LS, Heibert A, Causey PW, Christendat D, Lever ABP. Red manganese phthalocyanines from highly hindered hexadecaalkoxyphthalocyanines. Inorganica Chimica Acta 2006;359:2690–9.
[15] Stillman MJ, Nyokong T. In: Leznoff CC, Lever ABP, editors. Phthalocyanines: properties and applications, vol. 1. New York: VCH; 1989 (Chapter 3).
[16] Ozoemena K, Nyokong T, Westbroek P. Self-assembled monolayers of cobalt and iron phthalocyanine complexes on gold electrodes: comparative surface electrochemistry and electrocatalytic interaction with thiols and thiocyanate. Electroanalysis 2003;15:1762–70.
[17] Wöhrle D, Eskes M, Shigehara K, Yamada A. A simple synthesis of 4,5-disubstituted 1,2-dicyanobenzenes and 2,3,9,10,16,17,23,24- *Octa*substituted phthalocyanines. Synthesis 1993;2:194–6.
[18] Perrin DD, Armarego WLF. Purification of laboratory chemicals. second ed. Oxford: Pegamon Press; 1989.
[19] Obirai J, Nyokong T. Synthesis, spectral and electrochemical characterization of mercaptopyrimidine-substituted cobalt, manganese and Zn (II) phthalocyanine complexes. Electrochimica Acta 2005;50:3296–304.
[20] Lever ABP, Wilshire JP, Quan SK. Oxidation of manganese(II) phthalocyanine by molecular oxygen. Inorganic Chemistry 1981;20:761–8.
[21] Janczak J, Kubiak R, Sledź M, Borrmann H, Grin Y. Synthesis, structural investigations and magnetic properties of dipyridinated manganese phthalocyanine, MnPc(py)$_2$. Polyhedron 2003;22:2689–97.
[22] Nyokong T. Electronic spectral and electrochemical behavior of near infrared absorbing metallophthalocyanines. Structure and Bonding 2010;135:45–87.
[23] Lever ABP, Milaeva ER, Speier G. In: Leznoff CC, Lever ABP, editors. Phthalocyanines: properties and applications, vol. 3. New York: VCH Publishers; 1993. p. 1.
[24] Nombona N, Tau P, Sehlotho N, Nyokong T. Electrochemical and electrocatalytic properties of α-substituted manganese and titanium phthalocyanines. Electrochimica Acta 2008;53:3139–48.
[25] Finklea HO. In: Bard AJ, Rubenstein I, editors. Electroanalytical chemistry, vol. 3. New York: Marcel Dekker; 1996.
[26] Pilloud DL, Chen X, Dutton PL, Moser CC. Electrochemistry of self-assembled monolayers of iron protoporphyrin IX attached to modified gold electrodes through thioether linkage. Journal of Physical Chemistry B 2000;104:2868–77.
[27] Matemadombo F, Durmuş M, Togo C, Limson J, Nyokong T. Characterization of manganese tetraarylthiosubstituted phthalocyanines self assembled monolayers. Electrochimica Acta 2009;54:5557–65.
[28] Matemadombo F, Griveau S, Bedioui F, Nyokong T. Electrochemical characterization of self-assembled monolayer of a novel manganese tetrabenzylthiosubstituted phthalocyanine and its use in nitrite oxidation. Electroanalysis 2008;20:1863–72.
[29] Sabatani E, Rubinstein I. Organized self-assembling monolayers on electrodes. 2. Monolayer-based ultramicroelectrodes for the study of very rapid electrode kinetics. Journal of Physical Chemistry 1987;91:6663–9.
[30] Ozoemena K, Nyokong T. Voltammetric characterization of the self-assembled monolayer (SAM) of octabutylthiophthalocyaninatoiron(II): a potential electrochemical sensor. Electrochimica Acta 2002;47:4035–43.

[31] Porter MD, Bright TB, Allara D, Chidsey CED. Spontaneously organized molecular assemblies. 4. Structural characterization of *n*-alkyl thiol monolayers on gold by optical ellipsometry, infrared spectroscopy, and electrochemistry. Journal of American Chemical Society 1987;109:3559–68.
[32] Hutchison JE, Postlethwaite TA, Murray RW. Molecular films of thiol-derivatized tetraphenylporphyrins on gold: film formation and electrocatalytic dioxygen reduction. Langmuir 1993;9:3277–83.
[33] Kobayashi N, Janda P, Lever ABP. Cathodic reduction of oxygen and hydrogen peroxide at cobalt and iron crowned phthalocyanines adsorbed on highly oriented pyrolytic graphite electrodes. Inorganic Chemistry 1992;31: 5172–7.
[34] Zagal JH, Guilppi MA, Depretz C, Lelievre D. Synthesis and electrocatalytic properties of *Octa*alkoxycobalt phthalocyanine for the oxidation of 2-mercaptoethanol. Journal of Porphyrins and Phthalocyanines 1999;3: 355–63.
[35] Agboola B, Nyokong T. Synthesis and electrocatalytic properties of octaalkoxycobalt phthalocyanine for the oxidation of 2-mercaptoethanol. Analytica Chimica Acta 2007;587:116–23.
[36] Lyons MEG, Fitzgerald CA, Smyth MR. Glucose oxidation at ruthenium dioxide based electrodes. Analyst 1994;119:855–61.
[37] Bard AJ, Faulkner LR. Electrochemical methods: fundamentals and applications. USA: John Wiley & Sons Inc.; 2001.
[38] Caro CA, Bedioui F, Zagal JH. Electrocatalytic oxidation of nitrite on a vitreous carbon electrode modified with cobalt phthalocyanine. Electrochimica Acta 2002;47:1489–94.
[39] Pournaghi-Azar MH, Dastangoo H. Electrocatalytic oxidation of nitrite at an aluminum electrode modified by a chemically deposited palladium pentacyanonitrosylferrate film. Journal of Electroanalytical Chemistry 2004;567: 211–8.
[40] Santos WJR, Sousa AL, Luz RCS, Damos FS, Kubota LT, Tanaka AA, et al. Amperometric sensor for nitrite using a glassy carbon electrode modified with alternating layers of iron(III) *tetra*-(*N*-methyl-4-pyridyl)-porphyrin and cobalt (II) tetrasulfonated phthalocyanine. Talanta 2006;70:588–94.
[41] Tau P, Nyokong T. Electrocatalytic oxidation of nitrite by *tetra*-substituted oxotitanium(IV) phthalocyanines adsorbed or polymerised on glassy carbon electrode. Journal of Electroanalytical Chemistry 2007;611:10–8.